Development of a portable gamma imaging system for absorbed radiation dose control in targeted radionuclide therapy

Carlotta TRIGILA

PhD Student

Group IIRIC

(Instrument. & Imagerie Radio-isotopique Clinique)

L. Ménard, P. Lanièce , Y. Charon, M.-A. Duval, M.-A.Verdier, L. Ammour, A. Bricou

Radiation therapy

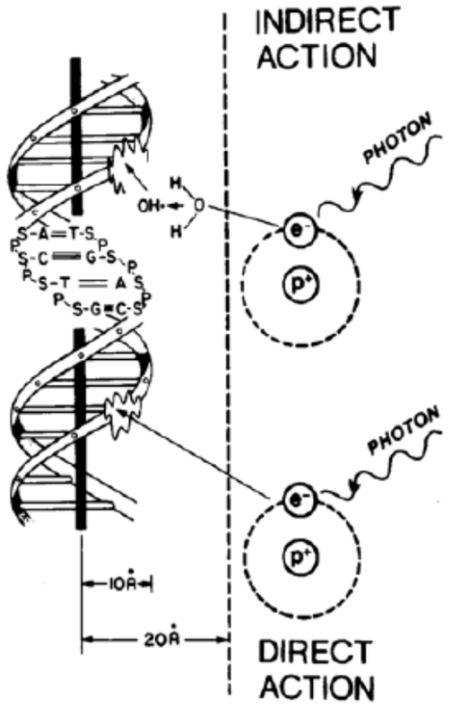

External Radiotherapy

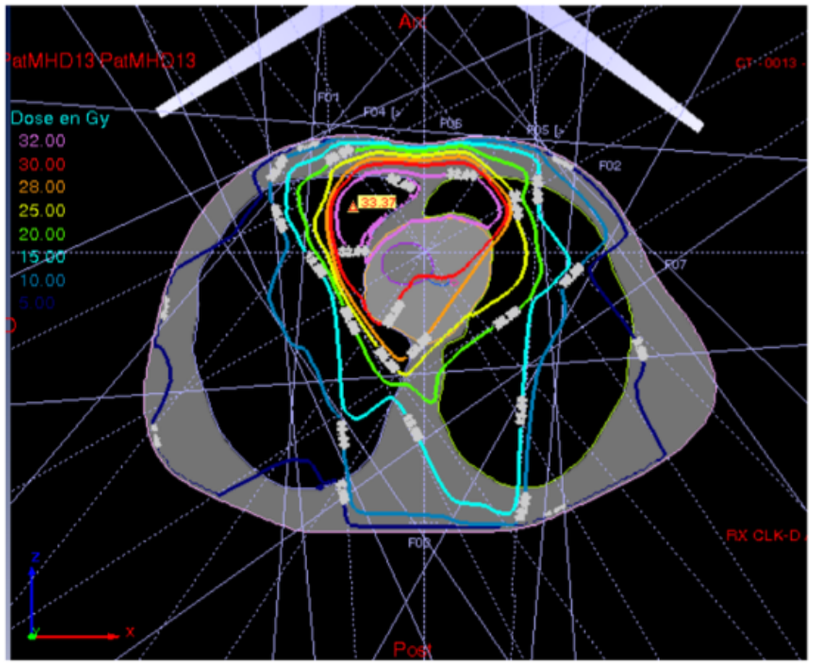

Internal Radiotherapy

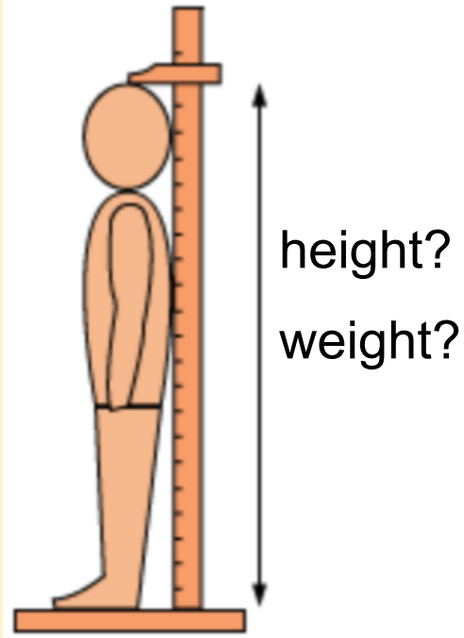

Targeted internal radiotherapy : local irradiation of tumors with alpha or beta emitting radionuclides ⟶ growing interest thanks to the emergence of new radiopharmaceuticals

Applications:

- **Differentiated thyroid cancer and benign thyroid disease (Graves disease, nodules)** ^{131}**I**
- Neuroendocrines tumors — ^{131}I-MIBG ou ^{90}Y/^{177}Lu-DOTADOC/DOTATATE
- Malignant lymphoma — ^{90}Y/14^{1}I-Anticorps monoclonal anti CD20
- Palliative treatment of the pains due to bone metastases — ^{89}Sr ou ^{153}Sm-biphosphonate
- Liver tumor — ^{90}Y-microspheres
- Prostate cancer with osseous metastases — ^{223}Ra

Control of the Dose

ELSEVIER MASSON

CrossMark

Disponible en ligne sur ScienceDirect www.sciencedirect.com

Elsevier Masson France EM|consulte www.em-consulte.com

Annales d'Endocrinologie 75 (2014) 241–246

Annales d'Endocrinologie
Annals of Endocrinology

Original article

Radioiodine therapy in benign thyroid disorders. Evaluation of French nuclear medicine practices

Abstract

Objectives. – Radioiodine is currently used routinely in the treatment of hyperthyroidism including Graves' disease (GD), toxic multinodular goitre (TMNG) and toxic solitary nodule (TSN) but no consensus exists on the most appropriate way to prescribe iodine – fixed dose or calculated doses based on the gland size or turnover of ^{131}I. We carried out the first nationwide French survey assessing the current practices in radioiodine treatment of hyperthyroidism. *Material and methods.* – A questionnaire was sent to French nuclear medicine hospital units and cancer treatment centres ($n = 69$) about their practices in 2012. *Results.* – Euthyroidism was considered the successful outcome for 33% of respondents, whereas hypothyroidism was the aim in 26% of cases. Fixed activities were the commonest therapeutic approach (60.0% of GD prescribed doses and 72.5% for TMNG and TSN), followed by calculated activities from Marinelli's formula (based on a single uptake value and thyroid volume). The fixed administered dose was chosen from between 1 to 3 levels of standard doses, depending on the patient characteristics. Factors influencing this choice were disease, with a median of 370 MBq for GD and 555 MBq for TSN and TMNG, thyroid volume (59%) and uptake (52%) with ^{131}I or ^{99m}Tc. Even physicians using fixed doses performed pretherapeutic thyroid scan (98%). *Conclusion.* – This study shows that practices concerning the prescription of ^{131}I therapeutic doses are heterogeneous. But the current trend in France, as in Europe, is the administration of fixed doses. The study provides the baseline data for exploring the evolution of French clinical practices.

Observations :

- big differences in the observed effects (response and toxicity)
- effects are dependent on the dose delivered to the tissues

Personalized dosimetry is essential for the optimization of the treatment (increase the dose in the tumor while sparing other organs)

Personalized Dosimetry

Needs of a dosimetry based on quantitative imaging of the biodistribution and kinetics of the radiopharmaceutical for each patient

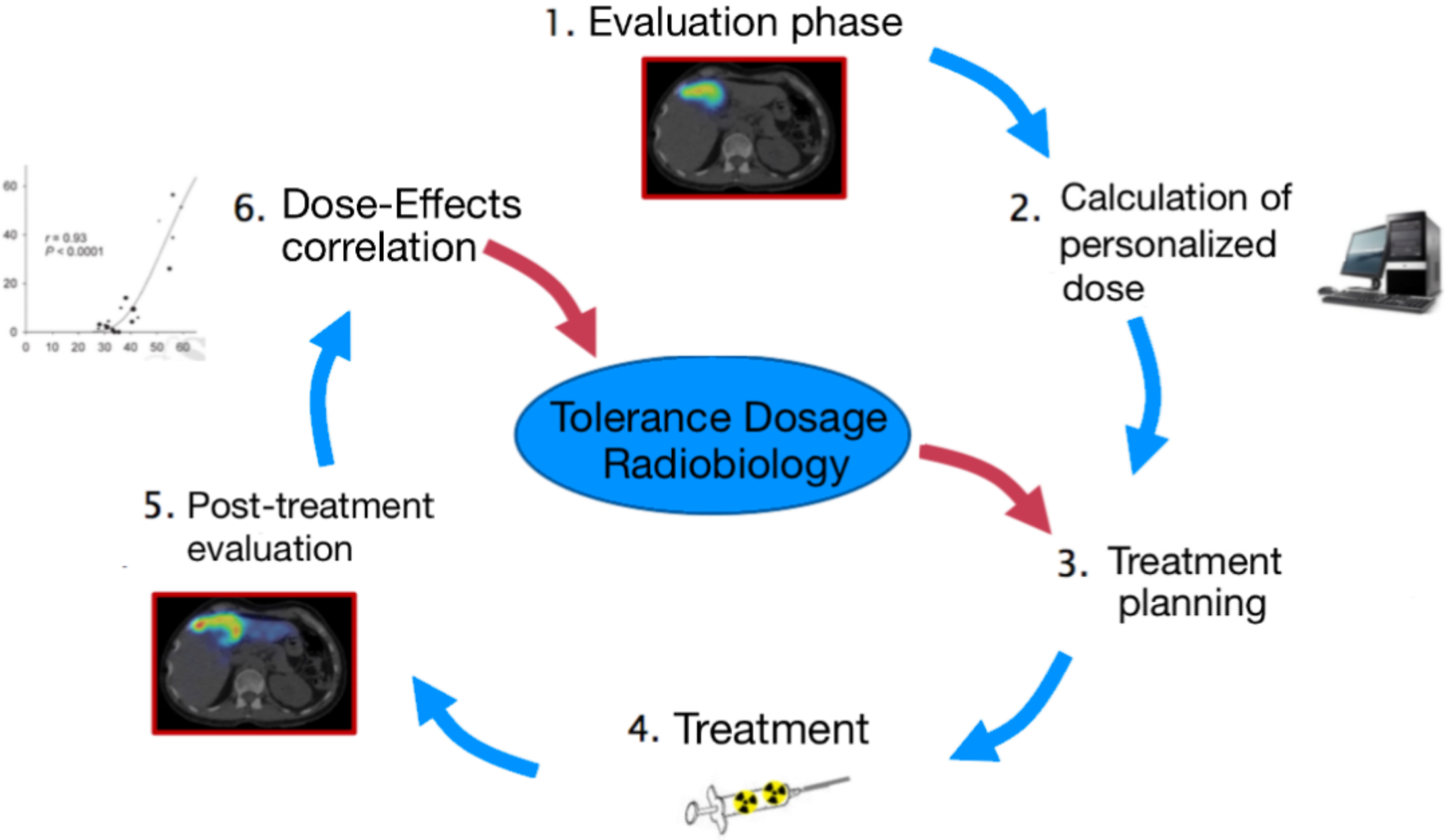

Personalized Dosimetry

Needs of a dosimetry based on quantitative imaging of the biodistribution and kinetics of the radiopharmaceutical for each patient

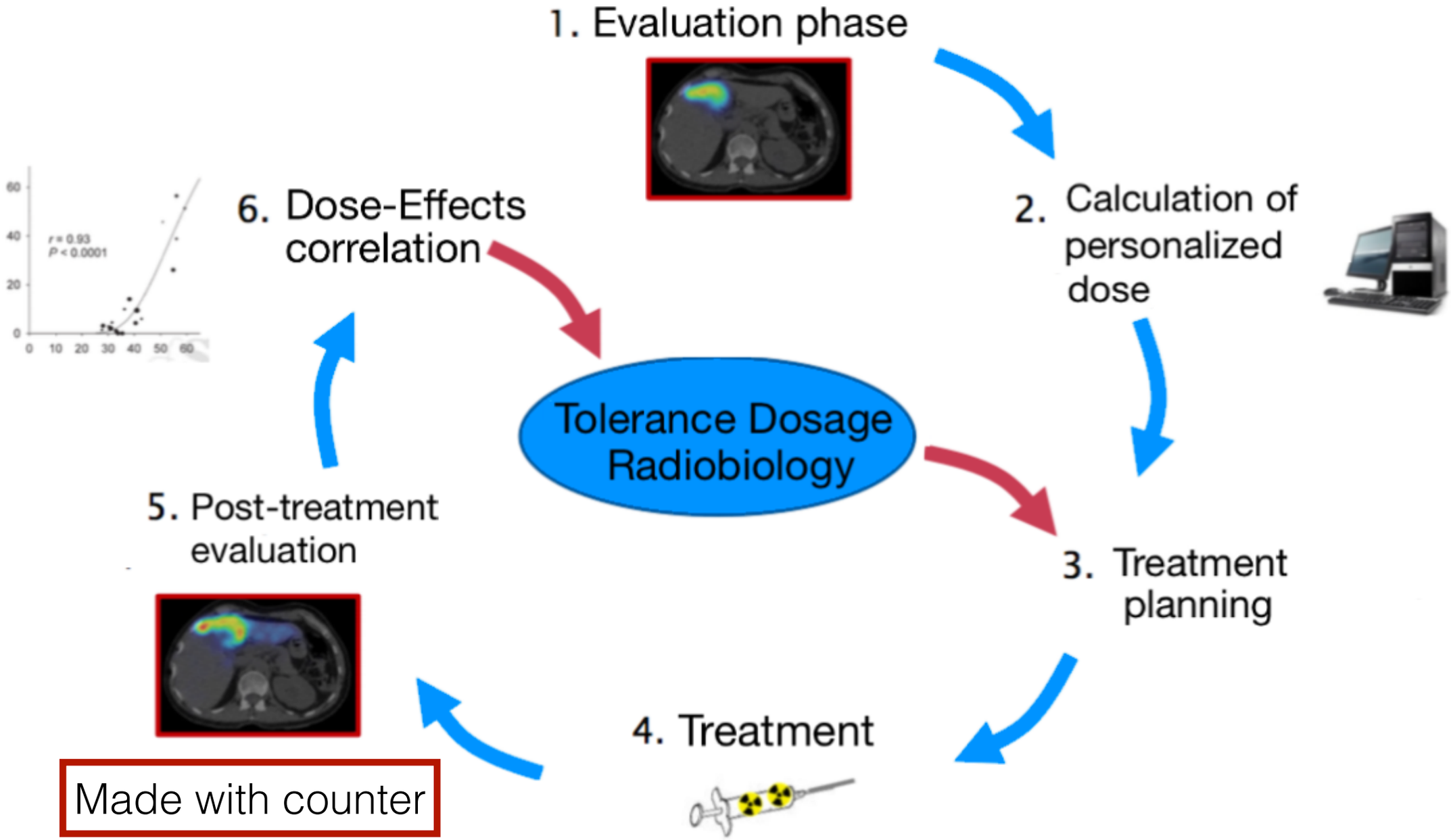

No imaging during the treatment

Challenges

- Development of imaging systems for quantitative measurements of absorbed doses delivered to the tumor and to the organs at risk *during the treatment :*

  - Correlation between the absorbed dose in the tumor/organ and the consequent clinical effects → optimization of the protocol in an iterative way

  - Control of the optimal dosage to be deposited during fractionated treatment

  - Study of the stunning effect (pre-therapeutic or self-stunning)

- Detection Constraints :

  - High energy gamma rays (>300 keV)

  - High fluxes

  - Exams performed in an isolated room at the patient's bedside

MoTi : Mobile Therapy Imager

- **Final purpose : develop a 10x10 cm² field of view mobile gamma camera dedicated to absorbed radiation dose control**

- Miniaturized gamma camera composed by :

  - parallel-hole high-energy tungsten collimator

  - continuous inorganic scintillator

  - 256 channels photodetection system

Photodetection system

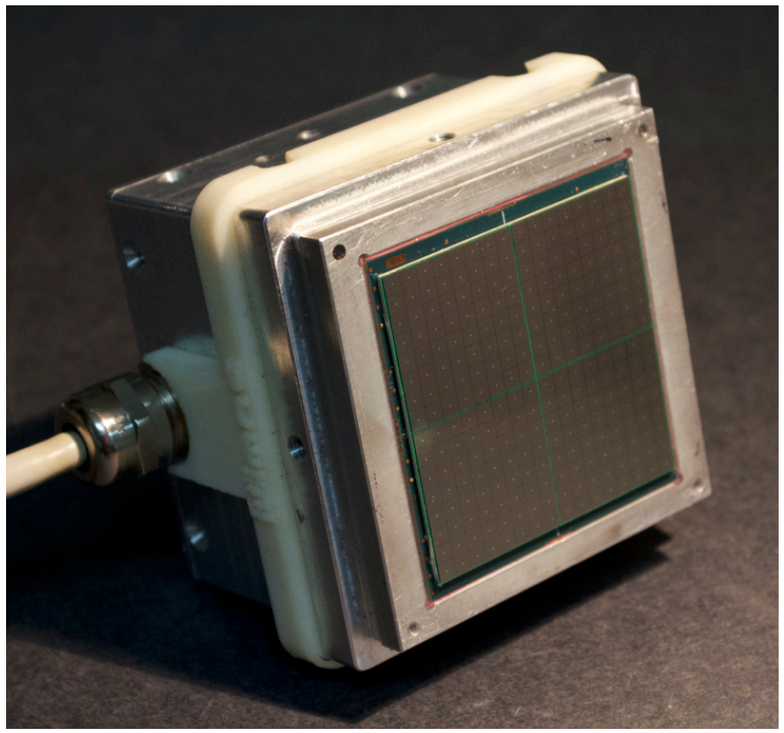

Architecture of the camera

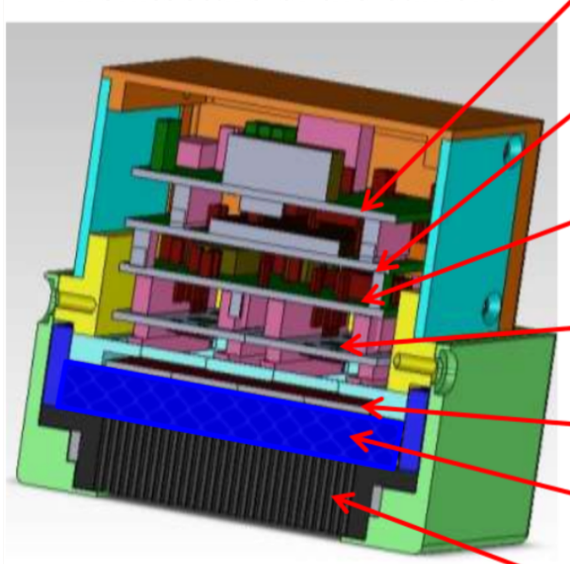

Development's axes

- **Definition and optimization of the detection head of the miniaturized camera (scintillator and collimator) in terms of spatial and energy resolution, efficiency and cost.**
  - ✓ Experimental characterization of different inorganic scintillators
  - ✓ Theoretical studies: rely both on the design of the collimator with analytical models and Monte Carlo simulation (GATE) and the optimization of the overall camera with numerical phantoms
- **Integration of a fully operational 5x5cm^2 camera prototype**

Development's axes

- **Definition and optimization of the detection head of the miniaturized camera (scintillator and collimator) in terms of spatial and energy resolution, efficiency and cost.**

  ✓ Experimental characterization of different inorganic scintillators

  ✓ Theoretical studies: rely both on the design of the collimator with analytical models and Monte Carlo simulation (GATE) and the optimization of the overall camera with numerical phantoms

- **Integration of a fully operational 5x5cm^2 camera prototype**

- **Characterization and optimization of the camera intrinsic properties**

Implementation of advanced reconstruction algorithm, correction of temperature dependencies

- **Image correction and quantification**

Attenuation and scatter, partial volume effect, compensation of the detector response function, background subtraction (Monte Carlo simulation with numerical phantom)

- **Biomedical validation :** Benign thyroid diseases/hyperthyroidism (^{131}I)

Scintillator-photodetector assemblies: insight

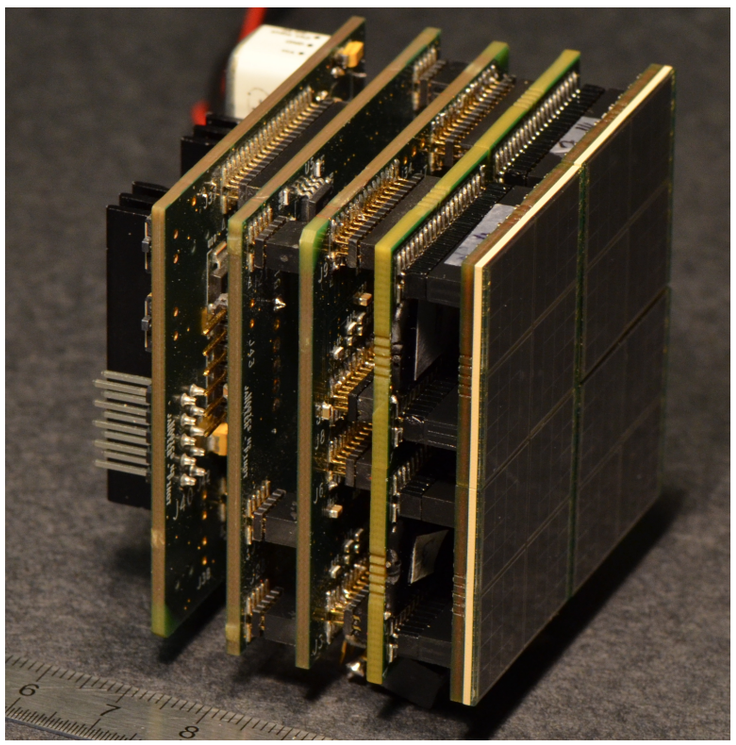

Photodetection system

256 SiPMs array (3x3 mm^2 SiPMs, 50x50 μm^2)

Four 64 channels ASIC/ADC modules (LAL, pôle OMEGA):

- Two 32 channels EASIROC ASICs
- External ADC (12 bits and 2Msamples/s)

Two 256 channels motherboards combining FPGA, USB interface and power supplies

Scintillator-photodetector assemblies: insight

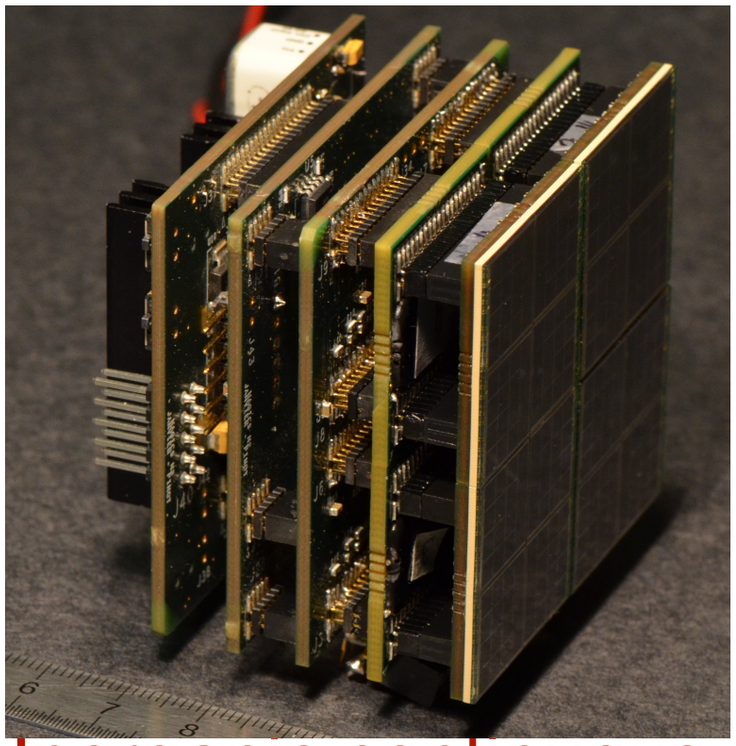

Photodetection system

256 SiPMs array (3x3 mm^2 SiPMs, 50x50 μm^2)

Four 64 channels ASIC/ADC modules (LAL, pôle OMEGA):

- Two 32 channels EASIROC ASICs
- External ADC (12 bits and 2Msamples/s)

Two 256 channels motherboards combining FPGA, USB interface and power supplies

Inorganic continuous scintillateurs

- Crystals tested : GaGG, $CeBr_3$, LaBr(Ce), LYSO, LFS
- Thickness 6 mm et 1 cm
- Different Optical coatings: diffusive, reflective, absorbing

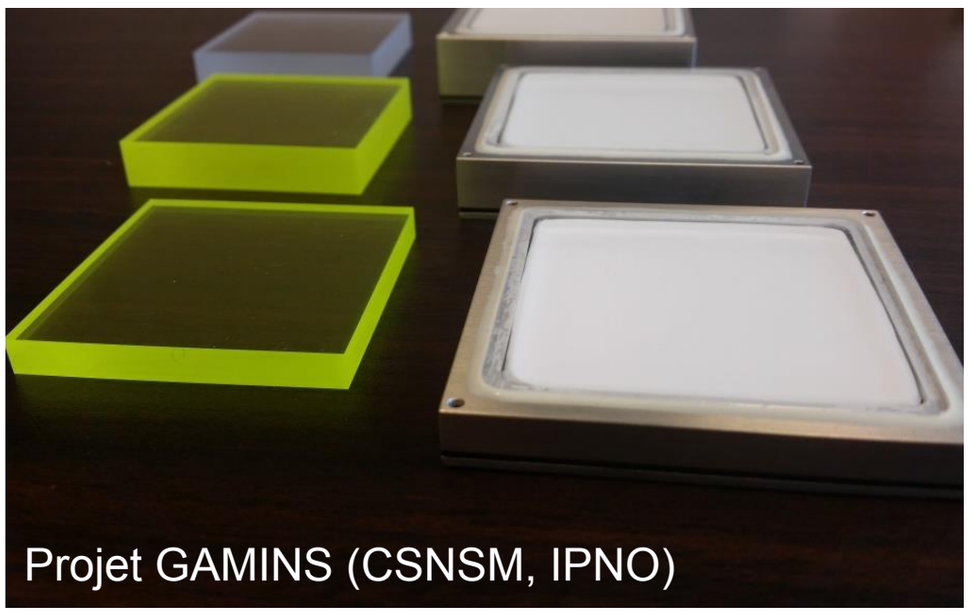

	Density (g/cm3)	Light Yield (ph/MeV)	Decay Constant (ns)	Refrax Index	Higroscopicity	Energy Linearity	Emission wavelength (nm)
LaBr:Ce	5,03	66000	18	2	Yes	100%	385
CeBr:Ce	5,18	60000	17	2,09	Yes	>100 KeV	370
LYSO:Ce	7,2	36000	33	1,81	No	>300 KeV	420
LFS	7,1	33000	40	1,81	No	>300 KeV	425
GAGG	6,63	55000	90-170	1,87	No	>200 KeV	520

Scintillator-photodetector characterization

Detector Spatial Response :

Study of uniformity response, linearity and spatial resolution

- ^{57}Co source
- 0.5 mm φ collimator
- 3 mm spaced spots (289 spots)

- Position of interaction reconstruction:
  - Scrimger-Baker Model
  - Levenberg-Marquardt algorithm

LaBr3:Ce 51 x 51 x 6 mm2
Absorbing edges

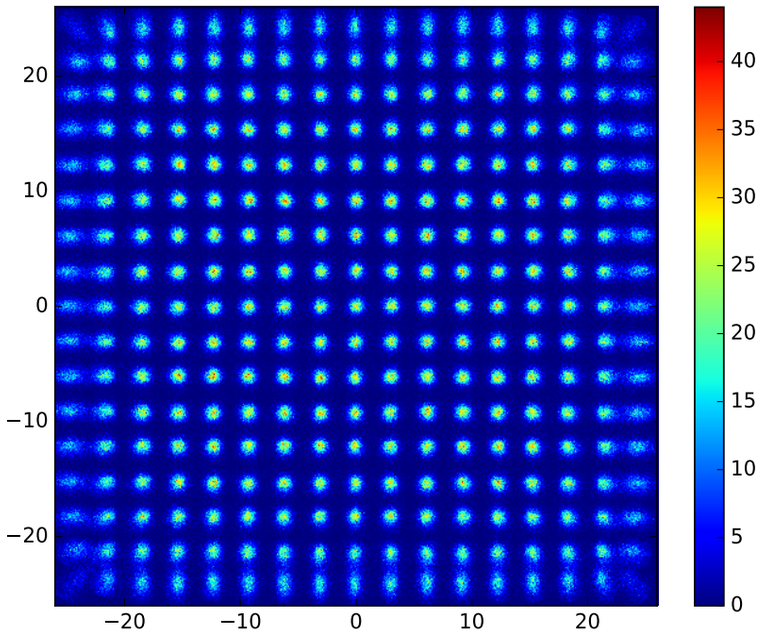

CeBr3 51 x 51 x 6 mm2
Absorbing edges

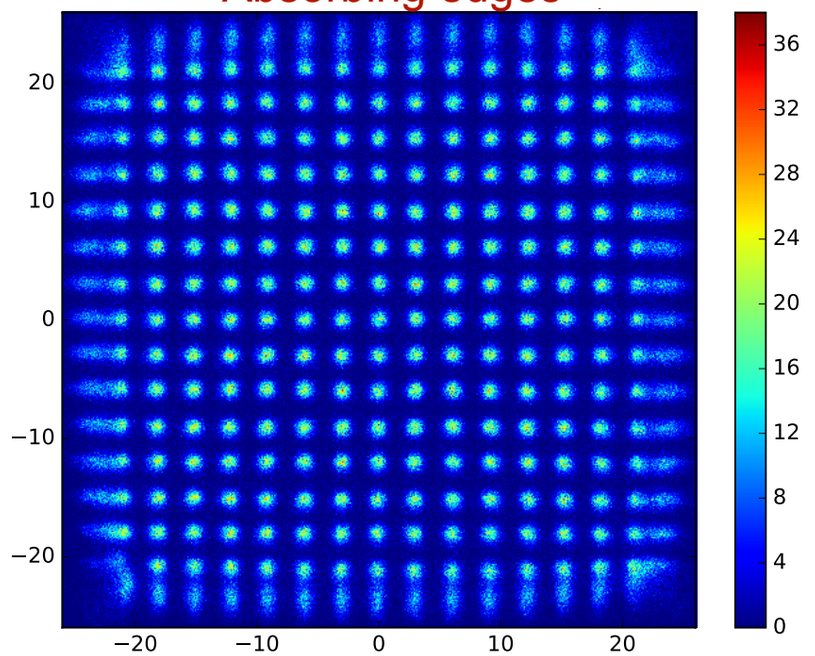

CeBr3
Average linear distortion(96% FoV)= 0.999

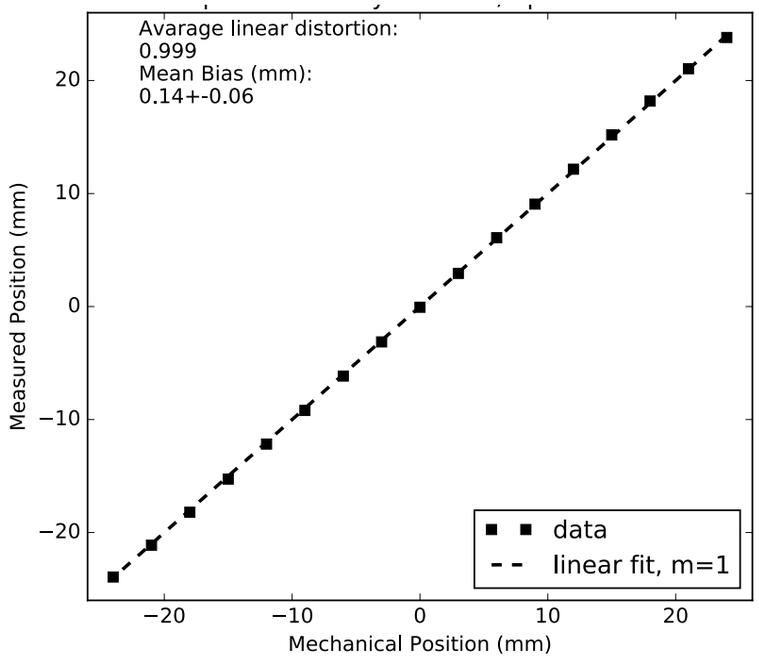

CeBr3
Spatial Resolution map

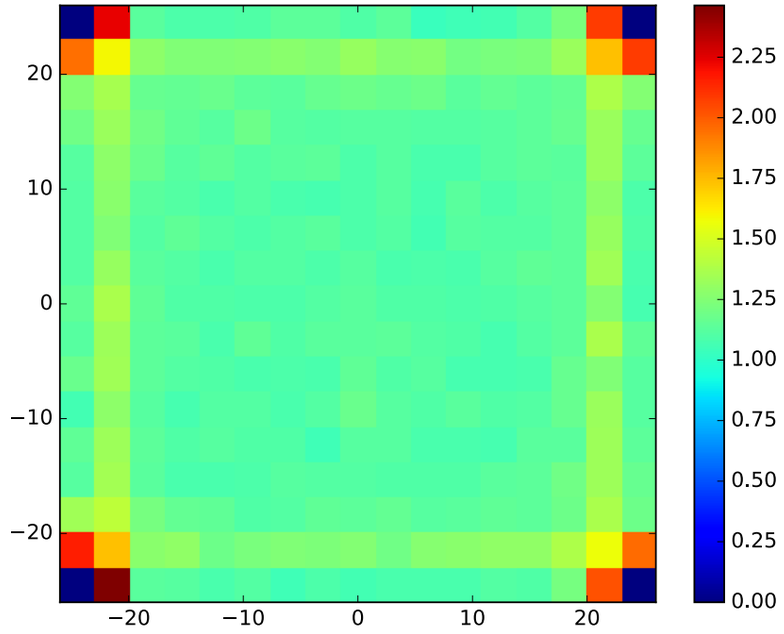

Scintillator-photodetector characterization

Spectrometric Properties

- ^{57}Co source
- 4 mm φ collimator
- 5 mm spaced spots (100 spots)

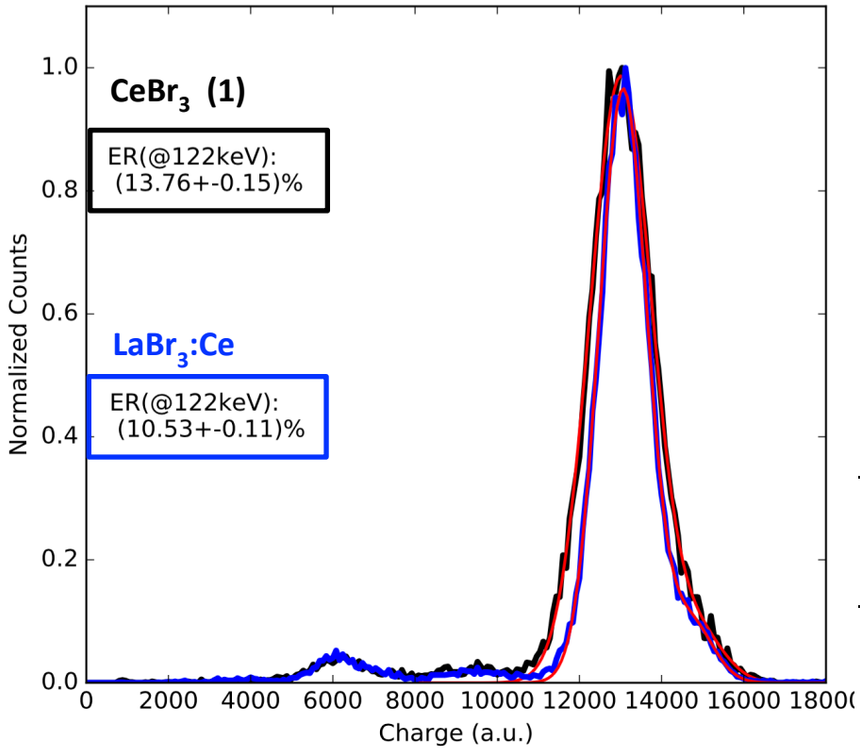

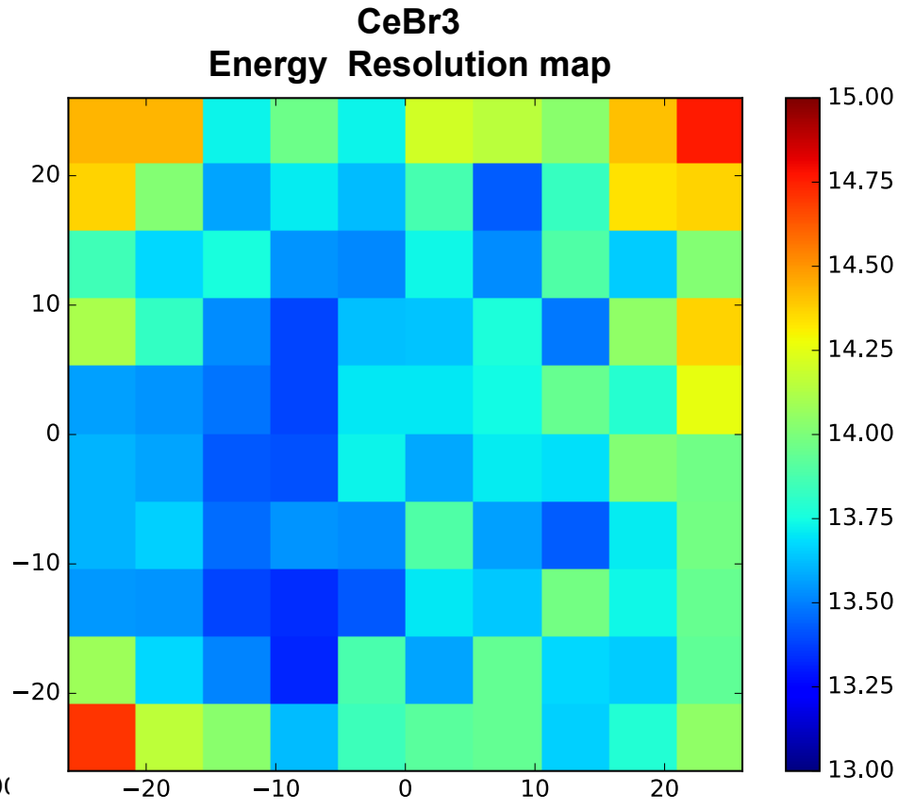

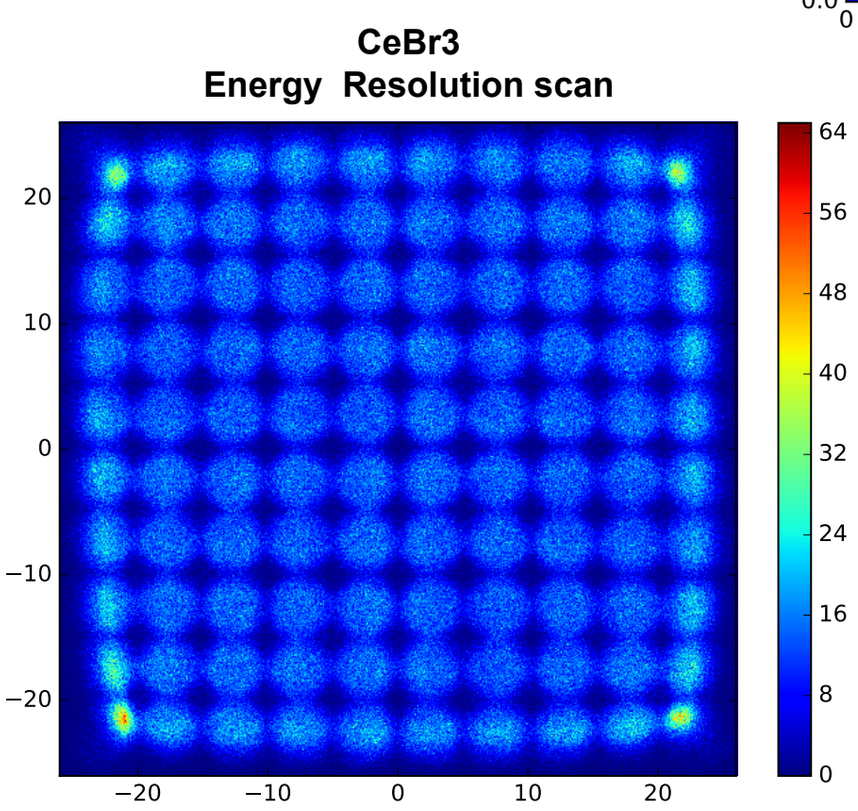

	LaBr$_3$:Ce	CeBr$_3$ (1)	CeBr$_3$ (2)
Dimensions (mm^3)	51x51x6	51x51x6	51x51x6
Optical Coating	Absorbing	Absorbing	Reflective
Light Guide (mm)	1	1.5	2
ΔE/E (%) @122 keV	10.68 ± 0.81	13.81 ± 0.30	12.40 ± 0.20
SR (mm)	1.00 ± 0.03	1.12 ± 0.03	1.34 ± 0.06
Bias (mm)	0.11 ± 0.09	0.13 ± 0.06	0.20 ± 0.08

Collimator intrinsic properties : Insight

Hexagonal parallel-hole high-energy tungsten collimator

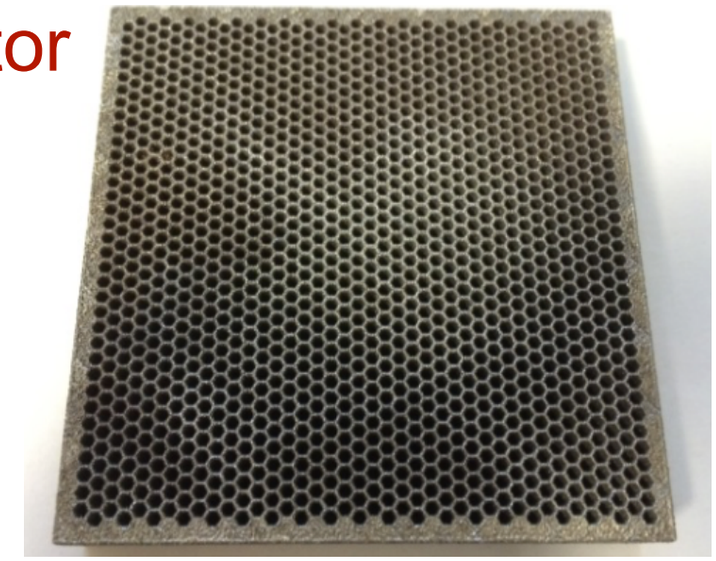

- Made with 3D printing (M&I Materials)
- Collimator geometry's optimization using both analytical model and MC simulations (GATE)
- Simulation of a 10x10 cm^2 field of view camera and a ^{131}I line source in air at a distance b = 5 cm

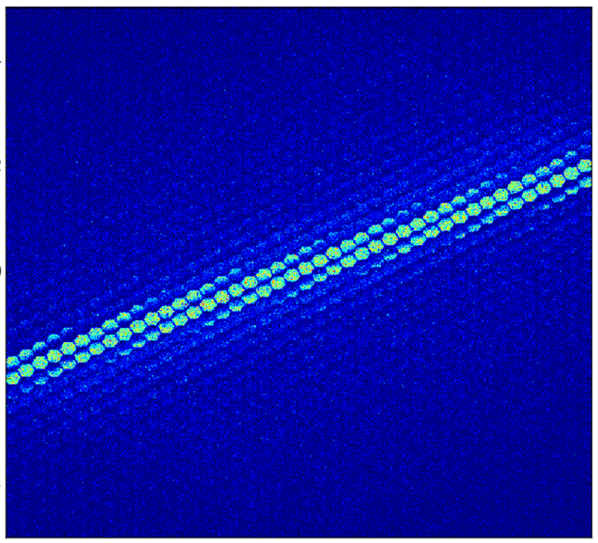

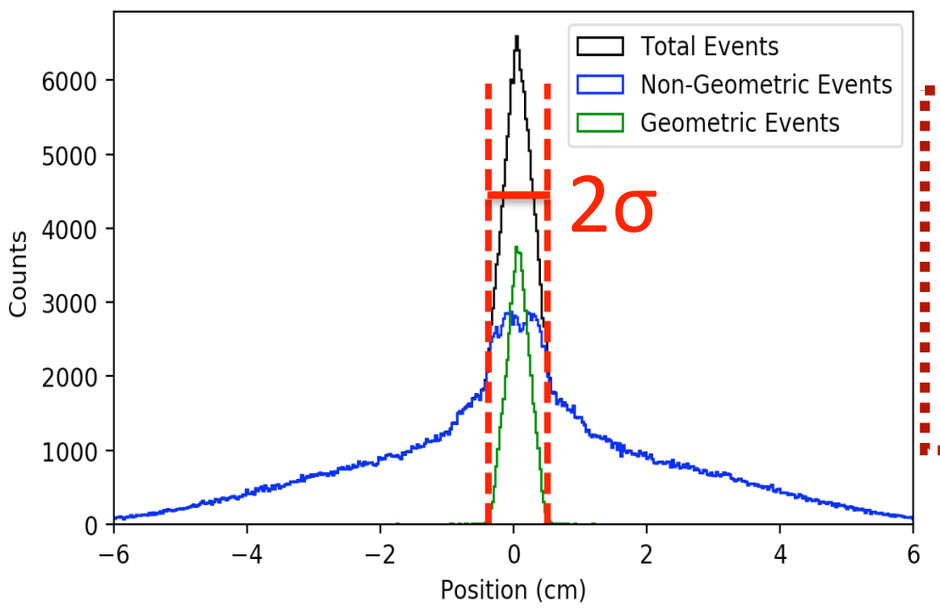

Configurations simulated:

- 8 thicknesses **L** ∈ [3,6.5] cm each 0.5 cm
- 8 diameters **d** ∈ [0.5,2.25] mm each 0.25 mm
- 12 septa **t** ∈ [0.75,2.125] mm each 0.125 mm

*Resolution (**R**)*:

From the σ of the profiles's sum inside vertical ROI through the line source

*Useful Efficiency (**uE**):*

Ratio between the counts inside 2σ and the events emitted

*Effective Septal Penetration (**eSP**):*

Ratio between the non-geometric events outside 2σ and the total events

Collimator intrinsic properties : Results

L=4.5 cm

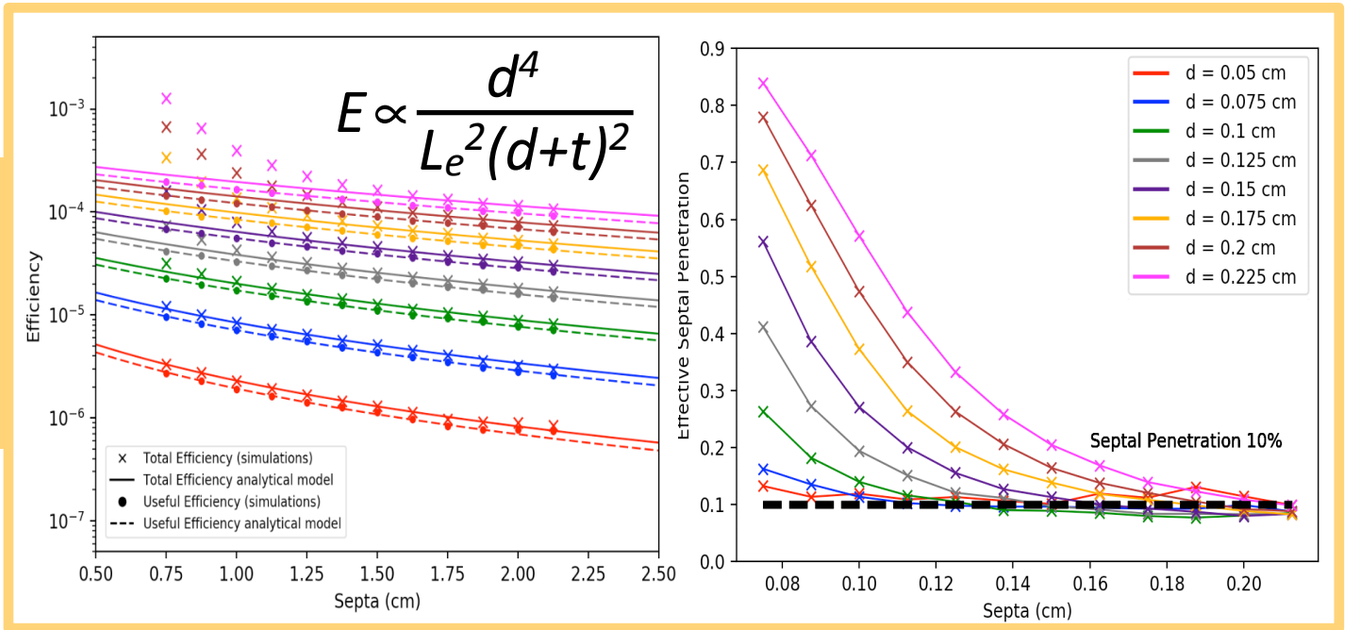

L=6.5 cm

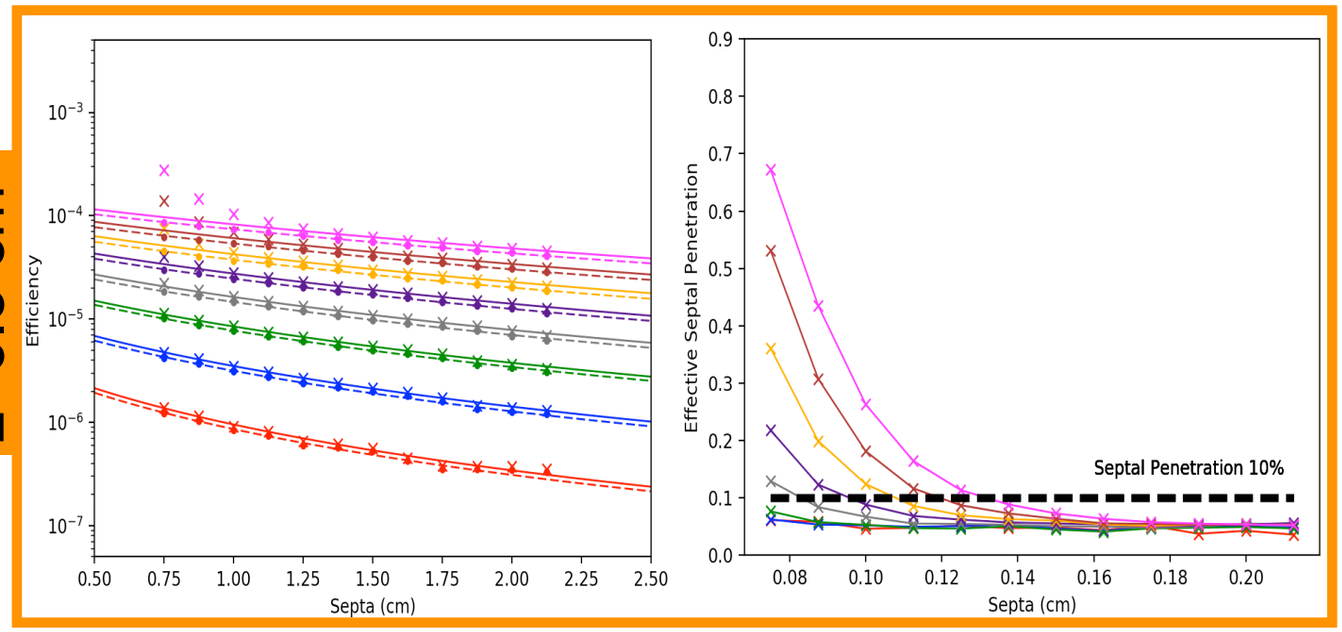

Collimator intrinsic properties : Results

L=4.5 cm

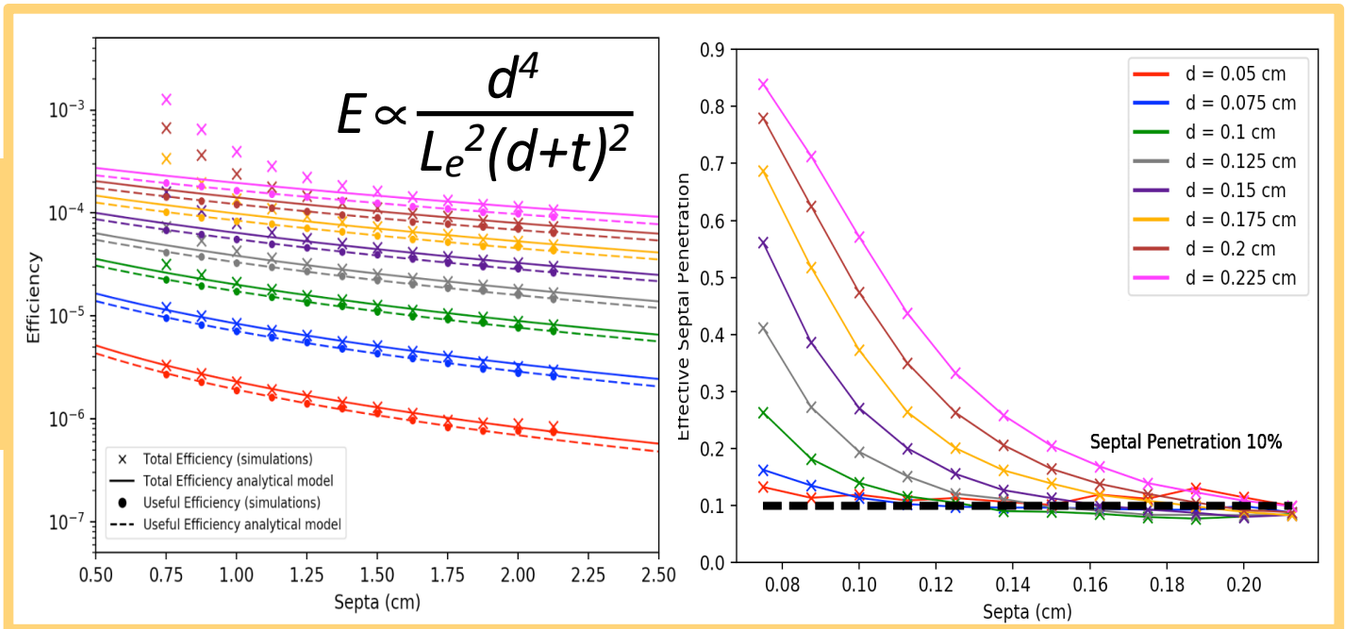

L=6.5 cm

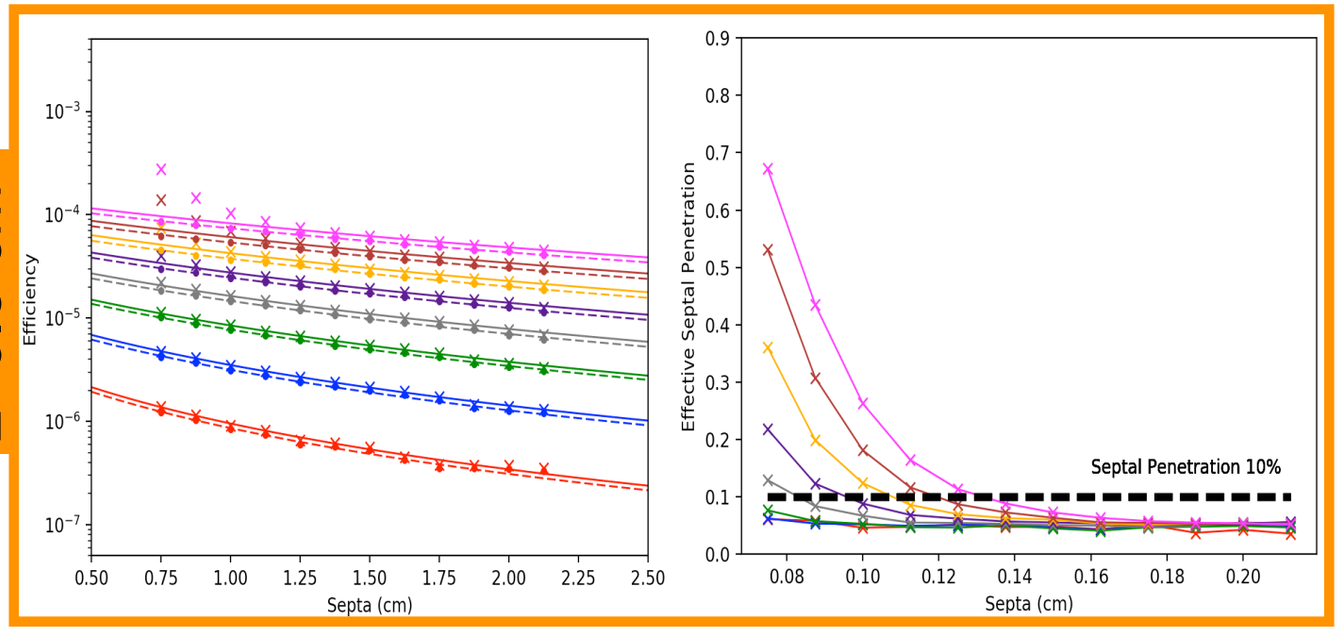

Final collimator configurations

- 5 configurations chosen using MC results and interpolation methods, with the constraint :

$$\mathbf{eSP = 10\%\ and\ SR \in [1,5]\ mm}$$

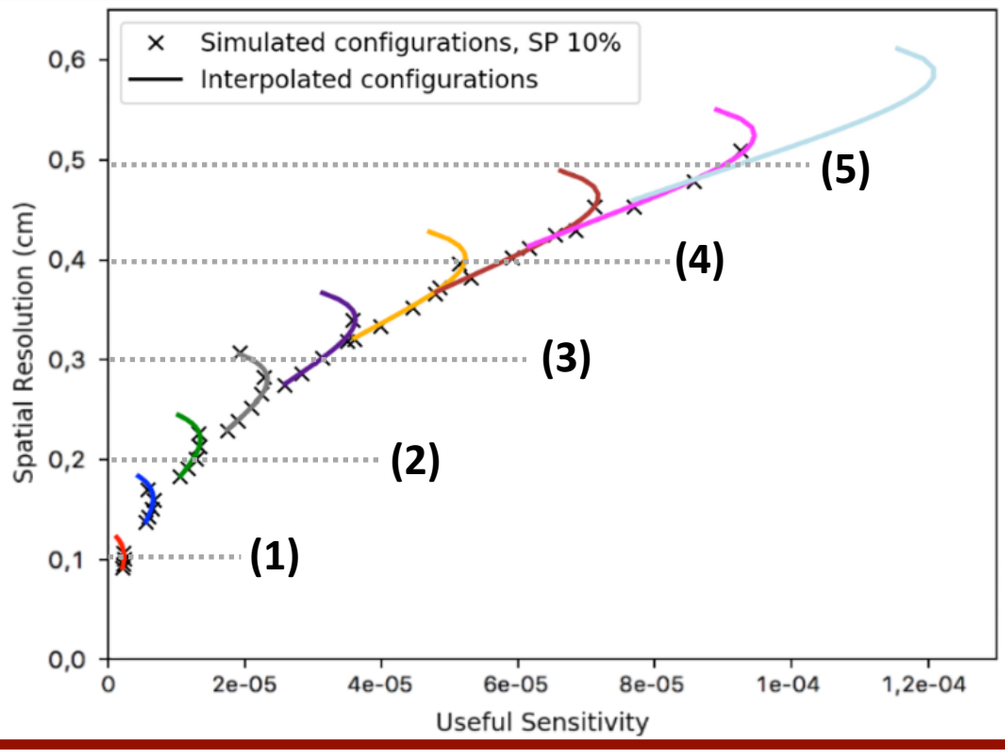

Configurations L=5,5 cm	(1)	(2)	(3)	(4)	(5)
d (cm)	0,05	0,1	0,15	0,2	0,25
t (cm)	0,055	0,085	0,115	0,145	0,175

Complete camera in a real clinical context

The final configuration's choice is realized simulating the complete camera in a real clinical context

- 2 cameras in conjugate view
- scintillators intrinsic properties used as simulation's input.
- Human phantom composed by three XCAT voxelized phantoms, for the head, the neck and the body

- Real hyperthyroidism activity distributions, 24h after ingestion of ^{131}I : nodules spread out (hot 6/12mm and 12 mm cold nodules) or thyroid diffuse hyper-functioning and enlargement

- Modeling of realistic background, coming from the radio-tracer uptake in surrounding normal organs, using a iodine bio-kinetics model

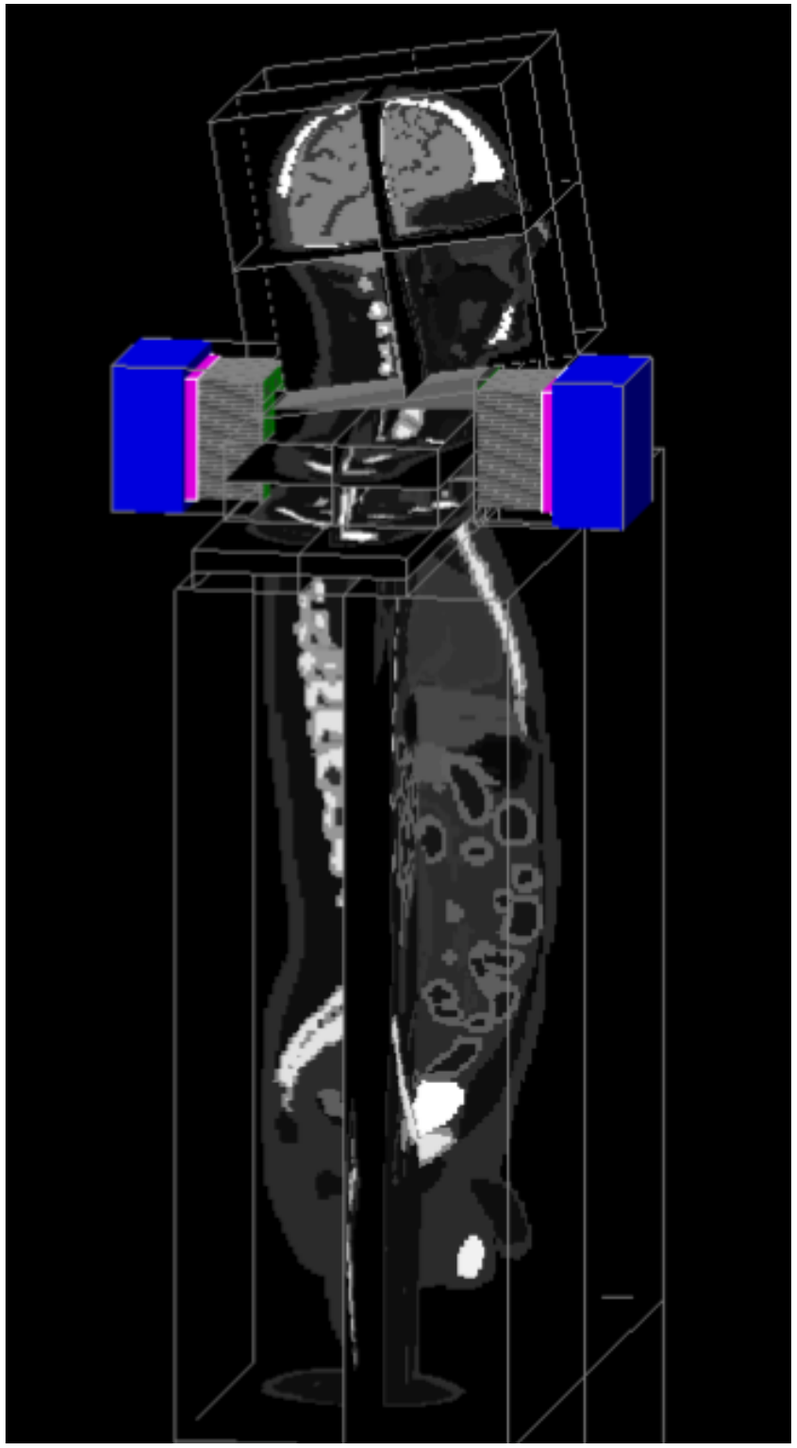

Complete simulation geometric overview: the two conjugate view and the XCAT human phantom.

Configuration choice : Preliminary Results

Estimation of nodules's activity using attenuation corrections according to MIRD 16

XCAT voxelized neck phantom slice
VOXEL= 1 mm²

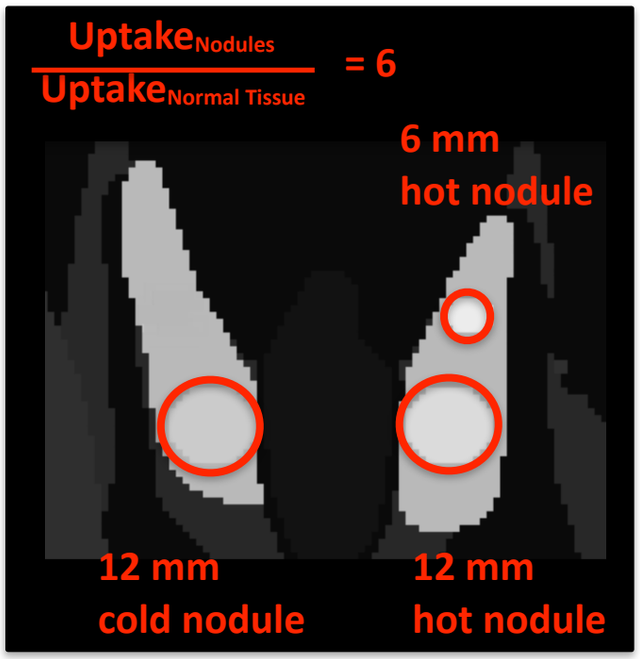

High-R/low-uE collimator (1)

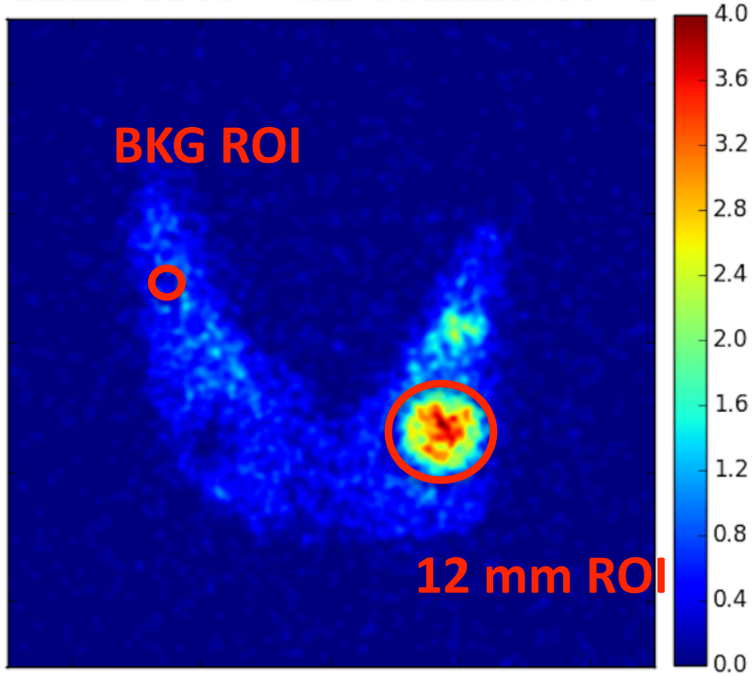

Mid-R/mid-uE collimator (3)

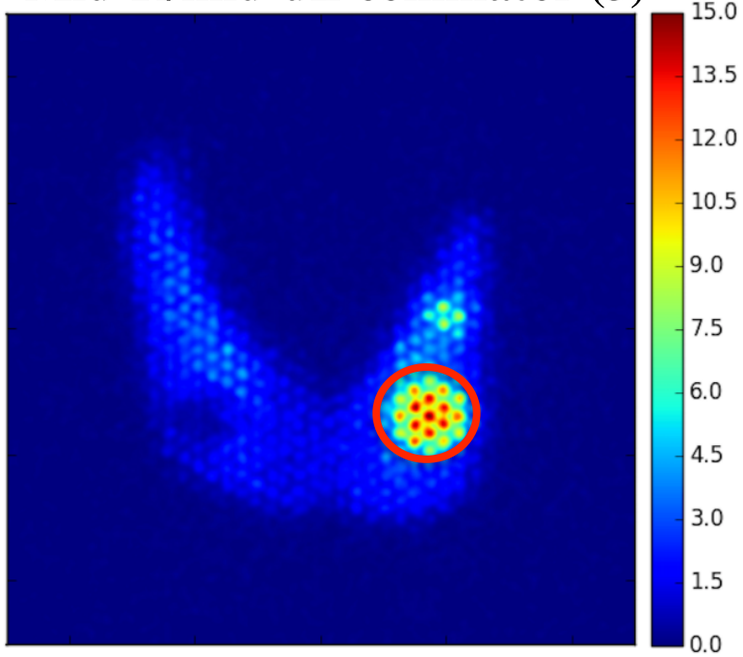

Low-R/high-uE collimator (5)

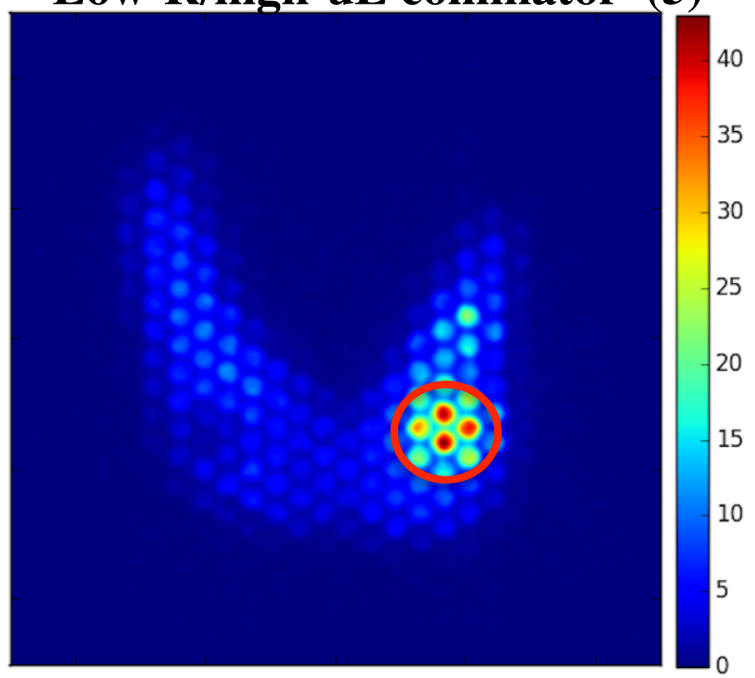

- Injected Activity = 600 MBq
- Thyroid Uptake = 55 %
- Acquisition Time = 1 min
- Images obtained with 6 mm $CeBr_3$
- ±10% energy window @ 364 keV

	Tot SR (mm)	Tot E	HBR	Δ Activity (%)
(1)	1,6	≃$5x10^{-7}$	34	31
(3)	3,2	≃$6x10^{-6}$	39	27
(5)	5,1	≃$1.75x10^{-5}$	41	31

- **Δ Activity** = Percentage difference between real and measured activity in the nodule
- **H** = Hot nodules counts in 12 mm ROI
- **BKG** = BKG counts in ten 20 mm² ROIs
- **SD** = BKG standard deviation
- **HBR** = H/BKG Hot-rod to BKG ratio

Conclusions and Next steps

- $CeBr_3$ seems to be a very good candidate for the specific need of the final prototype : good energy and spatial performances in the energy range of this application

- Detailed characterization of other fast inorganic crystal (LYSO, LFS and GaGG) is going underway

- Thanks to both analytical models and MC simulations, the choice of the best collimator geometry fall on collimators with 5.5 cm thickness, that allows septal penetration lower that 10% maintaining good imaging features

- Next step will concern the final choice of the best scintillator-collimator assembly and the integration of the complete 5x5 cm^2 prototype